Topographically Controlled Flow on the West Spitsbergen Shelf with special emphasis on the Atlantic Water transport towards Isfjorden

Frank Nilsen * , Juni Vaardal Lunde and Ragnheid Skogseth

The University Centre in Svalbard (UNIS), Longyearbyen, Norway

* *Corresponding author address:* Frank Nilsen, The University Centre in Svalbard (UNIS), P.O. Box 156, 9171 Longyearbyen, Norway

E-mail: frank.nilsen@unis.no. Phone: +47 79 02 33 38

ABSTRACT

A one layer numerical model is developed that demonstrates how the Atlantic Water (AW) from the West Spitsbergen Current (WSC) is topographically steered onto the West Spitsbergen Shelf (WSS) with a special emphasize on the Isfjorden Trough. Model results show that the WSC connects easier to the Isfjorden Trough than anywhere else on the shelf, letting the trough being exposed to warm and saline AW. The simple one layer barotropic model gives a good approximation of the dynamical processes on the WSS, which plays a significant role in the cooling process of the AW in the WSC on its way towards the Arctic Ocean. The intrusion of AW on Arctic shelves and into fjord systems also represents a transition from Arctic-type water masses to Atlantic-type water masses, and a complete change in the biomass and species composition. Estimates of oceanic heat transport on the WSS and towards the fjord system is presented. This heat has the potential to increase the melt rate of glaciers and has been identified as a likely mechanism leading to the acceleration, thinning and retreat of glaciers along the west coast of Spitsbergen.

1. Introduction

One of the more striking features of the large-scale ocean circulation within the Nordic Seas and Arctic Ocean is undoubtedly the way the currents trace out the shape of the underlying ocean basins (Nøst and Isachsen 2003). As observed and reported over a hundred years ago by Helland-Hansen and Nansen (1909), even the surface flow follows the topographic features that form sub-basins, ridges and plateaus hundreds or even thousands of meters below. In eastern Fram Strait, the West Spitsbergen Current (WSC) is topographically guided and flows along the Barents Sea continental slope with streamlines of f/H (Coriolis parameter/water column depth) and has been traditionally described as a barotropic flow along the Barents Sea and the West Spitsbergen Shelf (WSS) break (Aagaard et al. 1987; Manley 1995) (barotropic WSC branch in Teigen et al. (2010, 2011)). The major heat transport to the Arctic Ocean is through Fram Strait with the passage of Atlantic Water (AW) along the Svalbard margin in the West Spitsbergen Current (WSC) (Schauer et al. 2008). The Svalbard archipelago is situated in a climatically and oceanographically complex area. Warm AW in the WSC is generally isolated from the cold Arctic-type coastal waters by the Arctic Front (Saloranta and Svendsen 2001). Significantly heat is lost from the WSC as it flows northward through communication with the West Spitsbergen Shelf (WSS) (Saloranta and Haugan 2004; Nilsen et al. 2006). The continental shelf adjoining the west coast of Spitsbergen is complex, with alternating shallow banks (50-100 m depths) and deep troughs (200-400 m depths) cutting across the shelf. Cottier et al. (2007) examined the wind-driven circulation and upwelling on the WSS. Here we study the effect of varying the position of the WSC over the shelf break and focus on the circulation response on the WSS by developing a one layer model.

The present study focus on the Isfjorden Trough (Isfjordrenna) on the WSS, where the deep trough should have a significant signature on the mean circulation owning to the tendency to conserve potential vorticity. Repeated hydrographic cross section data, direct current measurements and results from a simple barotropic potential vorticity model presented here indicate that a steady, cyclonic, topographically trapped vortex resides over the Isfjorden Trough.

Section 2 introduce the study area and how the model grid is constructed. Section 3 goes through the quasi-geostrophic potential vorticity equation, how this equation can be solved numerically and how the equation connects to the WSS region. Results are presented and discussed in Section 4 and the paper is concluded in Section 5. The paper can easily be read without including the model theory Section 3, which is meant for modelers and researchers with a special interest.

2. The West Spitsbergen Shelf and the Isfjorden Trough

Fig. 1 shows the WSS including Van Mijenfjorden,Van Keulenfjorden, Kongsfjorden and the Isfjorden system. In Fig. 1 a, only the area that defines the model domain in Fig. 1 b is contoured with blue colors, the 500 m isobath defines the shelf break and the seaward boundary of the model domain. The troughs leading to the above mentioned fjord systems are included in the model domain while the fjord proper is not included in the model grid setup. The Isfjorden Trough can guide AW all the way from the WSC to the mouth area of Isfjorden (Nilsen et al. 2008). The deepest area of the WSS is found in the mouth of Isfjorden (Svensksunddypet) and the effect of this deep depression is included in the model as shown by the bottom contours in Fig. 1 b. The entrance to Isfjorden is behind this area, behind the coast line as described in Nilsen et al. (2008).

The grid is constructed of bathymetry from the WSS and fjord mouth areas based on the International Bathymetric Chart of the Arctic Ocean (IBCAO) (Jakobsson et al. 2008). For convenience, the y axis was located at the seaward boundary and was made a streamline to include the dynamic effect of the WSC. The 500 m bathymetry contour is chosen as the y axis where the contour meanderings are straightened to follow the y axis (Fig. 1a to Fig. 1b). Origin is placed at the 500 m isobath a little north of the South Cape latitude and the x axis is positive towards the coast line, where the coast line experience distortions due to the straightened 500 m isobath. Due to a very shallow region in the northern Forlandsundet, the island Prins Karls Forland is considered a peninsula attached to the West Spitsbergen coastline (Fig. 1b). This makes the boundary values easier to specify since the shoreline is assumed to be a streamline where $\psi = 0$.

Sectionss of temperature and salinity across and along the Isfjorden Trough are repeated twice every year (typically April and September) and the stations included in the Forlandet section are indicated by red dots in Fig. 1 a. Acoustic Doppler Current Profiler section from September 2010 show a nearly barotropic eastward current on the southern side of the trough (Fig. 2), while a more baroclinic westward current can be found on the northern side. The stratification in the WSS is generally weaker during winter and spring, and Fig. 3 confirms this for the Forlandet section collected in April 2011. The southern side of the section is filled with Atlantic Water (salinity above 34.9) from the surface to the bottom of the water column, and the water is guided eastward (towards the coast) along the southern trough slope. A vertical front between the colder and less saline shelf water can be seen towards Station 196. Modified AW and coastal water close to freezing point temperature are seen to flow seaward on the northern side of the section. Despite the apparent baroclinic structure, the flow seems to be guided by topography on the northern side as well, which indicate a geostrophic balance where the surface elevation plays the major role for the shelf and trough circulation pattern.

3. Hypothesis - A simple shelf flow model

The data constitute an example of the Taylor-Proudman effect (Taylor 1917; Proudman 1916), which is likely to occur in the ocean under appropriate conditions. This theory holds that steady flow in a rotating, constant-density fluid does not vary along the axis of rotation or, equivalently, that barotropic, geostrophic flow follows isobaths. The effect is modified by nonlinearity, stratification and viscosity.

In describing the initiation of stratified Taylor-Proudman columns, we utilize several scaling parameters that are here applied to the WSS to assess the relevance of the theory. Table 1 list the appropriate scales and scaling parameters. Most important are the Rossby number (ε) and the Ekman numbers (E_h, E_v), all of which must be very small for the lowest-order steady flow to be geostrophic. On the WSS it appears that $E_v^{1/2} \sim \varepsilon$, so that both advection and Ekman suction should be of similar importance. The data from the WSS indicate a cyclonic, or positive, vortex over a deep trough and anticyclonic flow around

a shallow bank; a pattern consistent with the conservation of potential vorticity. For this reason this study uses an inviscid potential vorticity model.

A steady, non-dimensional, barotropic, inviscid, quasi-geostrophic potential vorticity equation in an f-plane can be derived by expansion of the momentum and continuity equations in powers of ε (see e.g. Pedlosky (1987)) to yield

$$(\frac{\partial\psi}{\partial x}\frac{\partial}{\partial y} - \frac{\partial\psi}{\partial y}\frac{\partial}{\partial x})(\nabla^2\psi + \eta_B) = 0, \tag{1}$$

where ψ is the geostrophic stream function, or non-dimensional sea level, defined by $u = -\partial\psi/\partial y$, $v = \partial\psi/\partial x$; and η_B is given by $\eta_B = (h_B/\varepsilon D)$, where h_B is the height of the bottom above the reference depth D, as shown schematically in Fig. 4.

This expression was derived by assuming h_B/D is small, or O(ε). As such it is a valid approximation for the lowest-order flow since it approached

$$(\frac{\partial\psi}{\partial x}\frac{\partial}{\partial y} - \frac{\partial\psi}{\partial y}\frac{\partial}{\partial x})\eta_B = 0 \tag{2}$$

for $h_B/D \rightarrow$O(1) (Pedlosky 1987). This is the well known results that when the topographic relief is large, geostrophic flow follows depth contours. The expression for potential vorticity, $\nabla^2\psi + \eta_B$, however, is valid only for small h_B/D. Therefore, (1) is only an approximation for potential vorticity conservation. Nevertheless, in the limit $h_B/D \rightarrow 1$, the potential vorticity is dominated by the topographic term that the effect of O(ε) terms would hardly be noticeable.

a. The Numerical Potential Vorticity Model

The inertial potential vorticity equation (1) was chosen because the data indicate potential vorticity conservation; equation (1) state that potential vorticity, $\nabla^2\psi + \eta_B$, is conserved along a streamline. An equivalent expression is

$$\nabla^2\psi + \eta_B = K(\psi), \tag{3}$$

where the potential vorticity is a function of ψ. The function $K(\psi)$ is a value that must be determined for each streamline. Equation (3) is a Poisson equation where $G(x, y; \psi) = (\eta_B - K(\psi))$ will be prescribed on the boundary of the (bottom topography) grid. The

finite difference scheme used to solve (3) incorporate a rectangular grid (75 x 35) with the j (row) and k (column) subscripts representing the y and x axes (Fig. 1). The grid spacing, $\Delta x = \Delta y$, is 4 km and the finite difference notation for (3) is

$$-\frac{1}{4}\psi^t_{j-1,k} - \frac{1}{4}\psi^t_{j,k-1} + \psi^{t+1}_{j,k} - \frac{1}{4}\psi^t_{j,k+1} - \frac{1}{4}\psi^t_{j+1,k} = \frac{\Delta x^2}{4}[\eta_{Bj,k} - K(\psi_{j,k})] = \frac{\Delta x^2}{4}G_{j,k}, \quad (4)$$

with $\psi^{t+1}_{j,k}$ denoting the nodal solution at a position (k, j) in the grid, indicated by the superscript $(t + 1)$ forward in the iteration sequence, while t indicates known values on the grid around the node. Equation (4) comprise a 5-point Gauss formula, and from the resulting set of equations, a square sparse coefficient matrix A can be generated for the internal nodes (those lying inside the area of interest). The problem is then reduced to solving a linear system

$$A\psi = \frac{\Delta x^2}{4}G, \quad (5)$$

where A is a square matrix bounded by the number of internal grid points or number of grid points within the boundary values.

b. Boundary conditions - The West Spitsbergen Current

The upper slope branch of the WSC can be described as a topographically guided barotropic jet flowing along contours of planetary potential vorticity f/H (where f is planetary vorticity and H is water depth) and is referred to here as the barotropic WSC branch (Teigen et al. 2011). On the basis of repeated conductivity-temperature-depth (CTD) sections across the shelf edge front, Saloranta and Svendsen (2001) found that there is no subsurface density front associated with the Arctic temperature-salinity front on the West Spitsbergen shelf and concluded that barotropic rather than baroclinic instability was responsible for cross-frontal exchange between the WSC and the shelf waters. In the steady state circulation model studied here, emphasis is put on how warm and saline water in the WSC is directly guided onto the shelf by following bottom contours. The WSC is the boundary condition at the seaward boundary of our model domain and is controlled and varied by changing its maximum current speed and the position of its maximum current speed. Analyses of the current meter data suggest that the current is asymmetrical (Teigen et al. 2010), with a sharper current shear on the shore side than on the ocean side (Fig.

5a). An asymmetric (but still differentiable) idealized current profile was therefore proposed in Teigen et al. (2010) constructed by multiplying a Gaussian profile with a sigmoid curve, yielding a skew Gaussian profile (Fig. 5). Sections across the West Spitsbergen Current taken with ship-mounted Acoustic Doppler Current Profilers (ADCPs) (Walczowski et al. 2005) also support this idea.

For monitoring purposes, measurements are required at the shelf break because the WSC properties must first broach the shelf break in order to be transported across the shelf. In our simplified version of the barotropic WSC branch, the y axis is a streamline and fixed at the seaward boundary on the 500 m isobath where the averaged position of the WSC maximum current is found (Teigen et al. 2010) (Fig. 1 and Fig. 5a). The x axis is the upstream (southern) boundary where a cross slope distribution of ψ_0 is imposed, representing the eastern half of the skewed WSC profile, so that the function $K(\psi)$ can be determined. The sea-level ψ_0 increase from the maximum current position towards the shelf where ψ is set to the reference level zero in the initial setup of the numerical iterations. The stream function ψ is only allowed to be negative in order to be coupled to the boundary current, the WSC. A parabolic function was used assuming $\frac{\partial^2\psi_0}{\partial y^2} = 0$ and $\frac{\partial^2\psi_0}{\partial x^2} = -\frac{\zeta_0 L}{V}$ at $y = 0$, where L is the length scale and V is the velocity scale representing the maximum current of the WSC. Making the current profile more general by assuming that the maximum WSC can vary and is found at $x = a$, and utilizing that $\psi_0 = 0$ at the coast $x = L_x$, we arrive at the following boundary condition along the x axis ($y = 0$),

$$\psi_0 = -\frac{1}{2}\frac{\zeta_0 L}{V}\left(x^2 - \left(\frac{L_x}{L}\right)^2\right) + \left(\frac{\zeta_0 a}{V} + 1\right)\left(x - \frac{L_x}{L}\right), \tag{6}$$

and from this:

$$v_{WSC} = \frac{\partial\psi_0}{\partial x} = -\frac{\zeta_0 L}{V}\left(x - \frac{a}{L}\right) + 1. \tag{7}$$

There exist a position $x_0 = \frac{V}{\zeta_0 L} + \frac{a}{L}$ on the shelf where the v_{WSC} profile (7) reach a zero northward velocity. But a more dynamical important zero crossing is where the sea surface elevation reaches the reference level $\psi_0 = 0$:

$$x_{\psi_0} = 2\left(\frac{a}{L} + \frac{V}{\zeta_0 L}\right) - \frac{L_x}{L}. \tag{8}$$

This position has to be far enough east for the sea surface elevation to broach the shelf break in order to generate any current on the shelf and in troughs, and thus, for properties in

the WSC to be transported across the shelf. Hence, the primary role of the WSC is to set the height of the sea surface material isopleths along the shelf slope. Whether or not these material isopleths broach the shelf break is then a consequence of local shelf-wide wind and the advected WSC strength V.

Two assumptions influence the physical interpretation of the model results: (1) The stream function ψ is only allowed to be zero or smaller than zero, and (2) we chose a constant relative vorticity ζ_0 for the upstream boundary condition at $y = 0$, i.e. a linearly decreasing WSC profile from the maximum current (V) and towards the zero crossing on the shelf. The first assumption control the sea surface elevation and the geostrophic velocities and formula for zero crossing (8) determines where and when the WSC set up a pressure gradient force on shelf areas. By choosing a constant relative vorticity in the second assumption we strongly simplify the true nature of the WSC (Fig. 5). As seen in Fig. 5 (a) and (b), the yearly averaged current profile is a skewed gaussian jet profile with a highly varying relative vorticity across the West Spitsbergen Slope. The constant relative vorticity chosen for our model is given by the dashed line in Fig. 5 (b), $\zeta_0 = 0.4782 \cdot 10^{-5}$, and represent the eastern part of the WSC profile (Fig. 5 (a)) that is most often in contact with the shelf areas. The exact value of ζ_0 is chosen such that the a linear current profile with a maximum current at $x = 0$ of $V = 20$ cms^{-1} (the yearly average in Fig. 5 (a)) is not able to be topographically steered into troughs and onto the WSS, as shown in Fig. 1b where the contour lines just follows the West Spitsbergen Slope (WSSl). This is achieved by letting the stream function ψ have a zero crossing before a grid point where a bathymetric contour of the troughs on the shelf approach the slope region. A small increase in V or a shift in the position a of V towards the shelf will immediately initiate currents in the troughs and this paper will study the development and dependency of the shelf flow on a and V. Fig. 5 (c) show that the barotropic WSC can extend further onto the shelf when V increase or shift towards the shelf, and this is captured in our simple linear velocity profile (7).

Solutions to (5) is found through Matlabs backslash command which is equivalent to a Gaussian elimination. Initially, all values of ψ is set to zero except at the boundaries ($j = 1$ and $k = 1$). Along $k = 1$, $\psi_{j,k}$ were computed according to (7), and then $\psi_{1,k}$ was set to $\psi_{1,1} = \psi_0(k)$ for all j to initialize the seaward boundary. For each successive iterations

by Gaussian eliminations a new $\psi_{j,k}^{t+1}$ is calculated from (4) based on older values. Since $K(\psi)$ is conserved along streamlines (3) the function $K(\psi_{j,k})$ is determined by searching along the upstream boundary for the particular value to which $\psi_{j,k} = \psi_0(k)$ and calculating $K(\psi) = -\frac{\zeta_0 L}{V} + \eta_B(j = 1, k)$ at that point k. Moreover, $K(\psi_{j,k})$ is then used to calculate $G_{j,k}$ in (5). After each iterations a fractional change is calculated based on the old values, and a solution is reached when the fractional change between iterations converges towards a small value.

4. Results and discussions

Here, we present model results where the simple linear current profile representation of the WSC (equation (7) and Fig. 5 a) is moved eastward onto the shelf. Thus, the position of maximum WSC velocity (0.20 m/s) will be moved up the slope and onto the shelf by increasing a in (7). To illustrate this we show two cases for a in Fig. 6 a and b, where the green line is the linear WSC profile at the southwestern boundary of the model domain. The maximum WSC velocity, represented by a black arrow, is shifted eastward by $a = 2$ km in Fig. 6 a, and 8 km in Fig. 6 b.

The barotropic model is pressure driven through a tilting ocean surface that acts throughout the water column and drives the ocean currents. The ocean surface is represented by the stream function ψ in the model and the blue line in Fig. 6 show two cases of a tilting ocean surface at the upstream boundary of the model domain. The spatial derivatives of the ocean surface gives the current (green line). Since we initiate every model run by setting $\psi = 0$ except at the southern boundary, and only allow less than zero and zero ψ-values, all the ψ-values on the right hand side of the vertical red line in Fig. 6 is disregarded and set to zero. Hence, it is only the negative values on the left hand side of the red line that are able to generate a current in the model. This determines which bottom contours (Fig. 6 c) that will be exited by the WSC and be able to guide the current onto the shelf. For $a = 2$ km shown in Fig. 6 it is only the model grid points (black dots) on the left side of the red line situated 11.9 km eastward from the shelf break (Table 2) that feel the WSC. If the WSC is forced even further onto the shelf as in Fig. 6 b ($a = 8$ km), shallower areas and

shallower bottom contours will be exposed to the WSC and are able to guide AW deeper onto the shelf. This is clearly illustrated in Fig. 7 a and c, corresponding to the boundary conditions in Fig. 6 a and b, respectively, where water masses from the WSC circulates a large numbers of troughs and shallower areas on the WSS when the maximum velocity of the WSC is moved further eastward.

Table 2 list some of the important model parameters and volume transports result in the Forlandet section (Fig. 1 and 2) as a function of a, the position of the maximum current in the WSC. The second column gives x_{ψ_0}, i.e. how far east the sea surface elevation of the WSC reaches onto the shelf (the position of the red line in Fig. 6). This dominates the final circulation pattern and Fig. 7 a, b, c and d shows this pattern for a =2 km , 3 km , 8 km , and 14 km, respectively. When $a = 2$ km the maximum velocity of the WSC has climbed up 50 m from the 500 m isobath (Fig. 6 a) and the WSC sea surface tilt is able to generate current in the Isfjorden Trough only. Deep bottom slopes are able to guide AW in (east) at the southern side of Isfjorden Trough and out (west) on the northern side. No currents are generated above depth contours more shallow that 200 m, and this is the reason for no AW transport into the Kongsfjorden Trough (Fig. 1) at this stage. Forcing the WSC further onto the shelf (Fig. 7 b with $a = 3$ km) initiate flow above the 200 m isobath and cyclonic flow pattern is also generated in the Kongsfjorden Trough.

Fig. 7 shows that the WSC connect easier to the Isfjorden Trough than anywhere else on the shelf. When increasing a in the model runs, Fig. 7 also show that the AW finds new routs into the trough toward Isfjorden. At $a = 3$ km (Fig. 7 b), all the AW circulates around Tampen (Fig. 1) and continues eastward on the southern side of the Isfjorden Trough. In Fig. 7 c, when $a = 8$ km, circulation is stronger in Eggbukta and some of the isobaths in Eggbukta leads into the Isfjorden Trough along Lexryggen. This pathway is captured by the Forlandet Section that now experience two major branches transporting AW. When $a = 14$ km (Fig. 7 d) the route from Eggbukta over Lexryggen seems to dominate the inflow of AW toward Isfjorden. At this stage the Kongsfjorden Trough is receiving modified AW directly from the Isfjorden Trough, and Bellsund in front of Van Mijenfjorden is also in connection with the WSC. Hence, the entire WSS can be influenced by the warm and saline AW if the WSC is forced far enough onto the shelf. Large scale wind forcing can bring the WSC onto

the shelf by changing the sea surface elevation (Nilsen and Vaardal Lunde 2012), and the winter of 2012 and 2006 in Svalbard became above average warm with no sea ice forming due to the topographic guiding of AW onto the shelf.

Fig. 8 shows the volume transport through km in three different cross section in the Isfjorden Trough when $a = 8$. Here, we focus on the middle section, the Forlandet Section, since this section seems to capture all the flow branches in the trough and gives a representative picture of the changes in the volume transport when the boundary values are changed. Table 2 gives an overview of the volume transport i the Forlandet Section (Fig. 1) for the different a cases. Column five list the eastward transport on the southern side of the Isfjorden Trough, column six the westward transport on the northern side, and the last column list the total transport in the section. It is seen that the eastward inflow, on the order of 0.01 Sv (1 Sv = 10^6 m^3s^{-1}), to the Isfjorden Trough increase with increasing a, i.e. an increasing circulation of AW from the WSC to the WSS. The inflow is nearly compensated by the outflow on the northern side of the trough, but the total volume transport shows a net positive inflow on the oder of 0.001 Sv. The total volume reaches a maximum (0.0026 SV) around $a = 8$ km (Fig. 8) and then decreases again. The explanation to this is given by the conservation of potential vorticity. When a is low, the circulation on the shelf follows the deep bottom contours in the troughs. The deviation from the reference depth D, h_B, is then small, and thus, η_B becomes small, and the relative vorticity term in (3) becomes more important. This will guide some of the incoming water masses to circulation around the deepest depressions along the path, as seen around the Svensksunddypet in the mouth of Isfjorden. The deficit in the westward flowing barotropic volume transport will probably be compensated by a westward baroclinic transport (Fig. 3) not included in our model.

When a increase beyond 8 km, the WSC water masses choose to follow shallower regions on the shelf (Fig. 7 d). The reason being that the trough slopes are steeper on the upper part of the slopes (Fig. 1) and the AW therefore is more easily guided over these bottom contours due to conservation of potential vorticity. Moreover, this is reflected in the decreasing total volume transport in Table 2 since it is less easy for the water to start circulation around depressions and shallows.

Heat transport is determined by the difference in temperature between the temperature

being advected into or out of a volume as compared to the local temperature or the temperature representative for the water masses being replaced. Thus, if Fig. 7 represents the averaged circulation pattern for four different winter seasons, it is obvious that the heat transport onto the WSS will be very different between these cases due to the circulation of AW from the WSC and the contrast between AW temperatures and the local Arctic type water temperatures. It is not uncommon with large interannual variations in sea ice cover and averaged oceanic- and atmospheric temperature around Svalbard, especially not on the west coast of Spitsbergen, so the different circulations patterns in Fig. 7 reflect different heat transport situations on the WSS for different years. A more detailed explanation on the forcing and changes in the WSC can be found in (Nilsen and Vaardal Lunde 2012).

Since WSC connect easier to the Isfjorden Trough than anywhere else on the shelf, there will often be situations like Fig. 7 on the WSS. During winter when the contrast between the 2-3^{o}C AW and the shelf water close to freezing point temperature is largest, the heat input from the WSC to the WSS is noticeable in the sea ice cover and air temperatures. Using the eastward barotropic volume transports given in Table 2, the eastward heat transports on the southern side of the trough can reach 0.2-0.4 TW for a between 2-8 km. It is interesting to follow this AW as it circulate in the Isfjorden Trough and estimate how much heat is released to the atmosphere on its way. By assuming no heat is lost to the surrounding water masses, and thus, all the heat is lost to the atmosphere, the heat loss over a test area marked by the black rectangle (approximately 200 km^2) in Fig. 8 can be estimated. Teigen (2011) estimated that the heat loss from the ocean to the atmosphere on the WSS reach -500 Wm^{-1} in winter. Using this heat loss over our test area, we estimate that the water masses cools approximately 1^{o}C from the left hand side (Forlandet Section) to the right hand side of the rectangle (the Isfjorden mouth). This is close to the measurements during April 2011 showing a temperature reduction by 2^{o}C over the same distance. It also indicates that the heat loss to the surrounding water masses cannot be neglected but instead account for around half the heat loss.

5. Conclusion

The position of the WSC over the shelf break is controlling the circulation on the WSS. The maximum current of the WSC is on averaged found over the 500 m isobath. If the WSC is forced eastward over the shelf with only a couple of km, AW starts to flow onto the shelf and the warm and saline water is guided into troughs and towards the fjords along the west coast of Spitsbergen. The WSC connect easier to the Isfjorden Trough than anywhere else on the shelf and the modeled eastward barotropic heat transports into the trough is estimated to be between 0.2-0.4 TW. Moreover, the calculations show that half of the heat loss in the AW in the Isfjorden Trough has to be due to heat loss to the surrounding water masses, while the rest is lost to the atmosphere.

Acknowledgments.

The authors thank the research vessel crews on R/V Håkon Mosby and R/V Lance and all the AGF214 and AGF211 students that participated on these cruises. A special thank you to Steinar Myking for technical assistance during the cruises and Tor Gammelsrød for never giving up the ADCP.

REFERENCES

Aagaard, K., A. Foldvik, and S. R. Hillman, 1987: The west spitbergen current: disposition and water mass transformation. *J. Geophys. Res.*, **92 (C4)**, 3778–3784.

Cottier, F., F. Nilsen, M. Inall, S. Gerland, V. Tverberg, and H. Svendsen, 2007: Wintertime warming of an Arctic shelf in response to large-scale atmospheric circulation. *Geophys. Res. Lett.*, **34 (L10607)**, doi:10.1029/2007GRL029 948.

Helland-Hansen, B. and F. Nansen, 1909: The Norwegian Sea. Its physical oceanography based upon the Norwegian Researches 1900-1904. *Report on Norwegian Fishery and Marine-Investigations*, **2**, 1–359.

Jakobsson, M., R. Macnab, L. Mayer, R. Anderson, M. Edwards, J. Hatzky, H. W. Schenke, and P. Johnson, 2008: An improved bathymetric portrayal of the arctic ocean: Implications for ocean modeling and geological, geophysical and oceanographic analyses. *Geophys. Res. Lett.*, **35**, L07 602, doi:10.1029/2008GL033520.

Manley, T., 1995: Branching of Atlantic Water within the Greenland-Spitsbergen Passage: An estimate of recirculation. *J. Geophys. Res.*, **100(C10)**, 20 627–20 634.

Nilsen, F., F. Cottier, R. Skogseth, and S. Mattsson, 2008: Fjord-shelf exchanges controlled by ice and brine production: The interannual variation if Atlantic Water in Isfjorden, Svalbard. *Continental Shelf Res.*, **28**, 1838–1853.

Nilsen, F., B. Gjevik, and U. Schauer, 2006: Cooling of the West Spitsbergen Current: Isopycnal diffusion by topographic vorticity waves. *J. Geophys. Res.*, **111 (C08012)**, doi:10.1029/2005JC002 991.

Nilsen, F. and J. Vaardal Lunde, 2012: A simple topographically controlled shelf circulation model - Intrusion of atlantic water on an arctic shelf, in prep.

Nøst, O. A. and P. E. Isachsen, 2003: The large-scale time-mean ocean circulation in the Nordic Seas and Arctic Ocean estimated from simplified dynamics. *J. Marine Res.*, **61**, 175–210.

Pedlosky, J., 1987: *Geophysical Fluid Dynamics*. 2d ed., Springer-Verlag, New York.

Proudman, J., 1916: On the motion of solids in a liquid possessing vorticity. *Proc. Roy. Soc.*, **A 92**, 408–424.

Saloranta, T. M. and P. M. Haugan, 2004: Northward cooling and freshening of the warm core of the west spitsbergen current. *Polar Res.*, **23 (1)**, 79–88.

Saloranta, T. M. and H. Svendsen, 2001: Across the Arctic front west of Spitsbergen: high-resolution CTD sections from 1998-2000. *Polar Res.*, **20 (2)**, 177–184.

Schauer, U., A. Beszczynska-Möller, W. Walczowski, E. Fahrbach, J. Piechura, and E. Hansen, 2008: Variation of Measured Heat Flow Through the Fram Strait Between 1997 and 2006. *Arctic-Subarctic Ocean Fluxes*, R. R. Dickson, J. Meincke, and P. Rhines, Eds., Springer, Netherland, Earth and Environmental Science, 65–85.

Taylor, G. I., 1917: Motion of solids in fluids when the flow is not irrotational. *Proc. Roy. Soc.*, **A 93**, 99–113.

Teigen, S. H., 2011: Water mass exchange in the sea west of Svalbard, a process study of flow instability and vortex generated heat fluxes in the West Spitsbergen Current. Ph.D. thesis, The University Centre in Svalbard and University of Bergen, Norway.

Teigen, S. H., F. Nilsen, and B. Gjevik, 2010: Barotropic Instability in the West Spitsbergen Current. *J. Geophys. Res.*, **115**, C07 016, doi:10.1029/2009JC005996.

Teigen, S. H., F. Nilsen, R. Skogseth, B. Gjevik, and Beszczynska-Mller, 2011: Baroclinic instability in the west spitsbergen current. *J. Geophys. Res.*, **116**, C07 012, doi:10.1029/2011JC006974.

Walczowski, W., J. Piechura, R. Osinski, and P. Wieczorek, 2005: The West Spitsbergen Current volume and heat transport from synoptic observations in summer. *Deep Sea Res. Part I*, **52 (8)**, 1374 – 1391, doi:10.1016/j.dsr.2005.03.009.

List of Tables

TABLE 1. Scales and scaling parameters appropriate to the West Spitsbergen Shelf and Slope

V	$\sim$	20-36 cm s^{-1}	Velocity scale (max current in the barotropic WSC)
L	$\sim$	80 km	Length scale (trough length and AW shelf penetration)
f	$=$	1.43×10^{-4} s^{-1}	Coriolis parameter ($\sim$78°N)
A_v	$\sim$	1×10^{-4} m^{-2} s	Vertical eddy viscosity
A_h	$\sim$	10 m^{-2} s	Horizontal eddy viscosity
D	$=$	500 m	Bottom depth at max WSC velocity
h_B^0	$\sim$	300 m	Characteristic trough hight
ε	$=$	$\frac{V}{fL} \sim$ 0.018-0.032	Rossby number
δ	$=$	$\frac{h_B^0}{D} \sim 0.6$	Trough aspect ratio
$1/2E_v^{1/2}$	$=$	$1/2(\frac{A_v}{fD^2})^{1/2} \sim 8.4\times10^{-3}$	Vertical Ekman number
$1/2E_h$	$=$	$1/2(\frac{A_h}{fL^2}) \sim 8.8\times10^{-5}$	Horizontal Ekman number

TABLE 2. Model parameter and Isfjordrenna volume transport across the Forlandet section

a [km]	x_{ψ_0} [km]	V [ms^{-1}]	ε	VT_E [m^3s^{-1}]	VT_W [m^3s^{-1}]	VT [m^3s^{-1}]
0	7.9	0.200	0.0175	0	0	0
0.5	8.9	0.202	0.0177	$1.061 \cdot 10^4$	$-1.051 \cdot 10^4$	$0.100 \cdot 10^3$
1.0	9.9	0.205	0.0179	$1.061 \cdot 10^4$	$-1.051 \cdot 10^4$	$0.100 \cdot 10^3$
2.0	11.9	0.210	0.0184	$1.061 \cdot 10^4$	$-1.051 \cdot 10^4$	$0.100 \cdot 10^3$
3.0	13.9	0.214	0.0188	$1.661 \cdot 10^4$	$-1.534 \cdot 10^4$	$1.264 \cdot 10^3$
4.0	15.9	0.219	0.0192	$1.661 \cdot 10^4$	$-1.534 \cdot 10^4$	$1.264 \cdot 10^3$
5.0	17.9	0.224	0.0196	$2.144 \cdot 10^4$	$-1.942 \cdot 10^4$	$2.029 \cdot 10^3$
8.0	23.9	0.238	0.0209	$2.652 \cdot 10^4$	$-2.395 \cdot 10^4$	$2.570 \cdot 10^3$
10.0	27.9	0.248	0.0217	$2.926 \cdot 10^4$	$-2.670 \cdot 10^4$	$2.561 \cdot 10^3$
12.0	31.9	0.257	0.0225	$3.054 \cdot 10^4$	$-2.849 \cdot 10^4$	$2.048 \cdot 10^3$
14.0	35.9	0.267	0.0234	$3.285 \cdot 10^4$	$-3.172 \cdot 10^4$	$1.127 \cdot 10^3$
16.0	39.9	0.276	0.0242	$3.465 \cdot 10^4$	$-3.425 \cdot 10^4$	$0.406 \cdot 10^3$

List of Figures

5 The time averaged (October 2007-June 2008) velocity profile (a) of the fitted skewed jet WSC profile construct from observations in the WSC across Fram Strait at 78.83^{o}N. The black arrow shows the maximum velocity in the WSC and the line marked by v_{WSC} is the function used to represent the WSC in the model. The calculated relative vorticty of the WSC is also shown (b). A fitted skew jet profile of the WSC, from October 2007 to June 2008, at the 200-250 m level at F0-F5, from Teigen et al. (2010). Mooring positions are marked in all figures and the mooring depth is given in brackets in (a). The vertical black line through all the subfigures marks the value chosen for the relative vorticity ζ_0 in the model. 27

6 The surface elevation (blue line) and corresponding WSC current (green line) representation in the barotropic model. The WSC current is moved eastward with $a = 2$ km in (a) and $a = 8$ km in (b) and the red line in each subfigure indicates the region on the WSS slope (c) that is affected by the WSC. The bottom profile in (c) represents the southern boundary of the model area where the WSC profile is prescribed. Black dots show the model grid and the vertical arrows show the position of the maximum WSC velocity. 28

7 The modeled circulation (a), (b), (c) and (d) where the maximum current of the WSC is translated an eastward distance a =2 km , 3 km , 8 km , and 14 km, respectively. Contoured streamlines/circulation pattern ψ (red lines) is plotted on top of the bottom topography (black lines). 29

8 Contoured streamlines/circulation pattern ψ (red lines) on top of the bottom topography (black lines). The blue curves show the volume transport across three different sections in the Isfjorden Trough when $a = 8$ km. The black rectangle marks a test area of approximately 200 km^2 that is used to calculate the effect of heat loss form the ocean to the atmosphere. 30

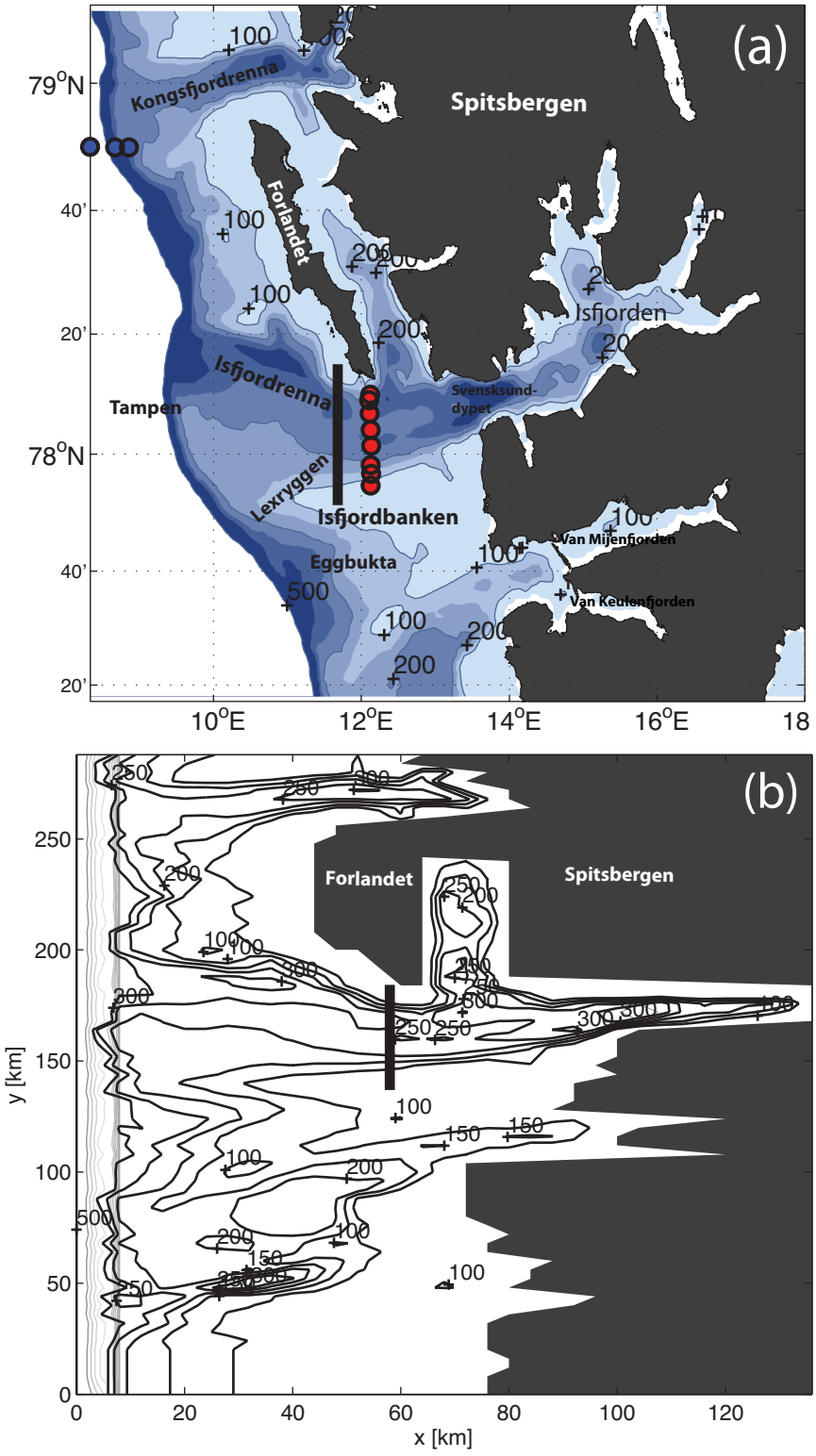

FIG. 1. Bathymetric map of the study area (a) based on the International Bathymetric Chart of the Arctic Ocean (IBCAO) (Jakobsson et al. 2008). In the model grid (b), the 500 m bathymetry contour is chosen as the y axis where the contour meanderings are straightened to follow the y axis. Origin is placed at the 500 m isobath a little north of the South Cape latitude and the x axis is positive towards the coast line.

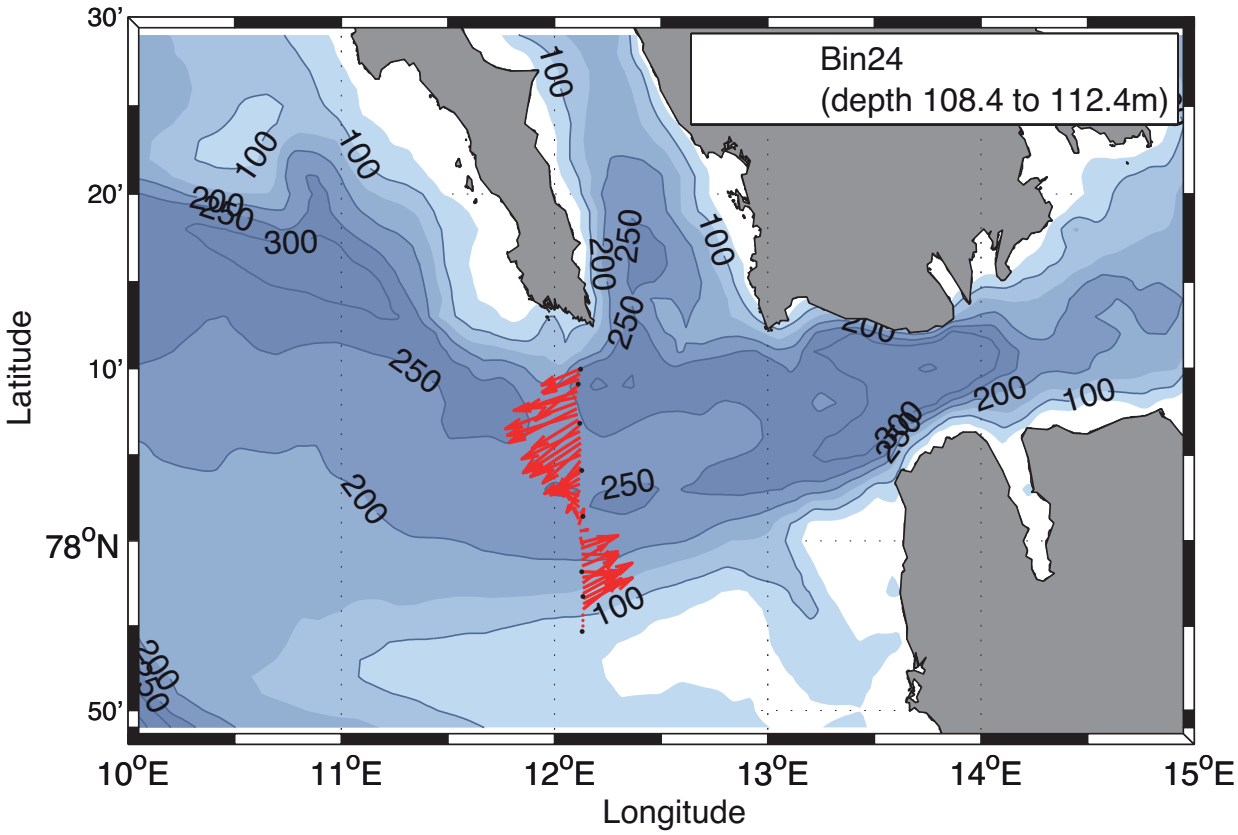

FIG. 2. Acoustic Doppler Current Profiler (ADCP) data collected in September 2010 from R/V Håkon Mosby. The horizontal currents in the Forlandet Section are shown for the depth bin at approximately 110 m.

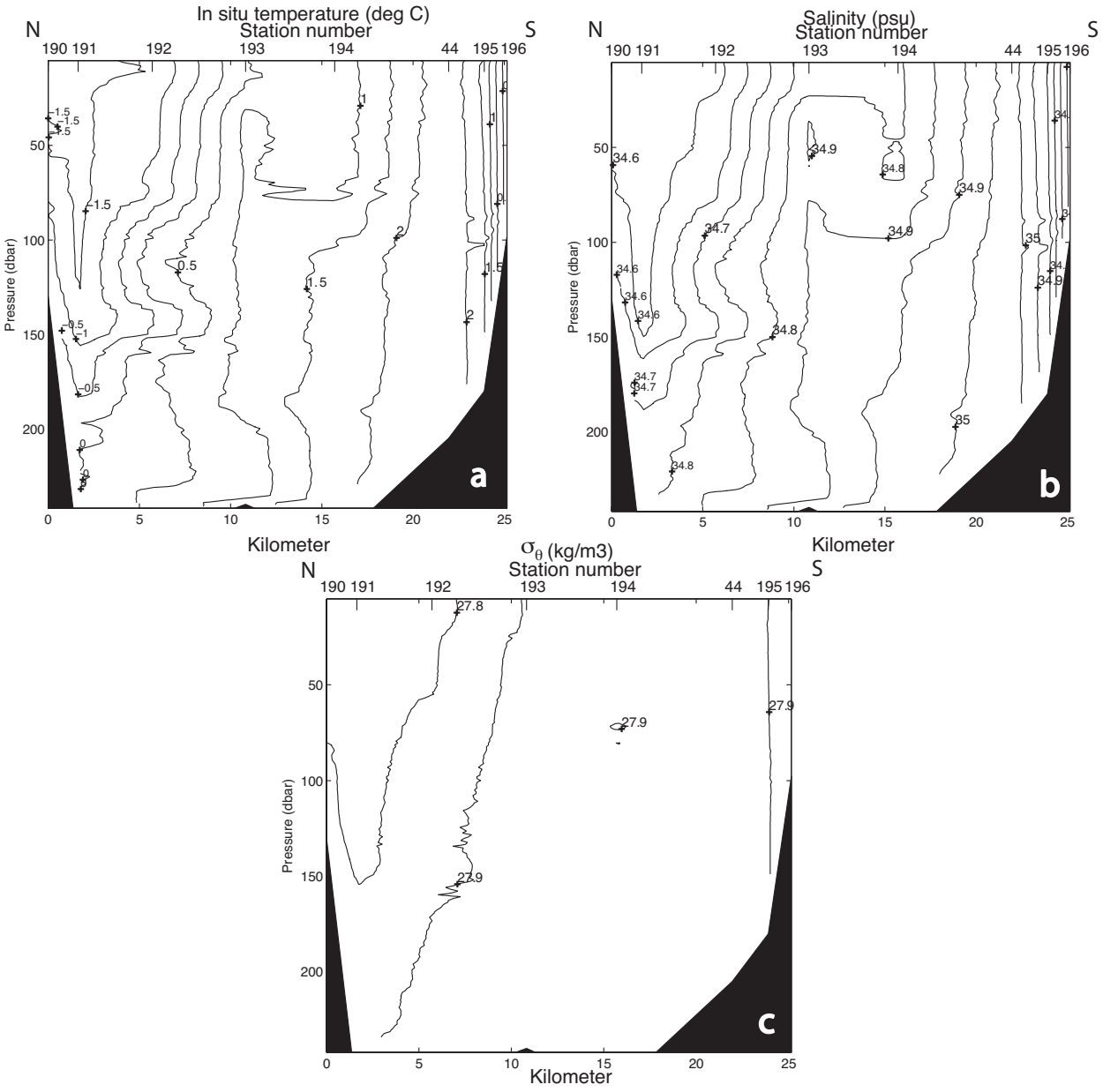

FIG. 3. Temperture (a), salinity (b) and potential density (c) in the Forlandet Section collected in April 2011 from R/V Lance.

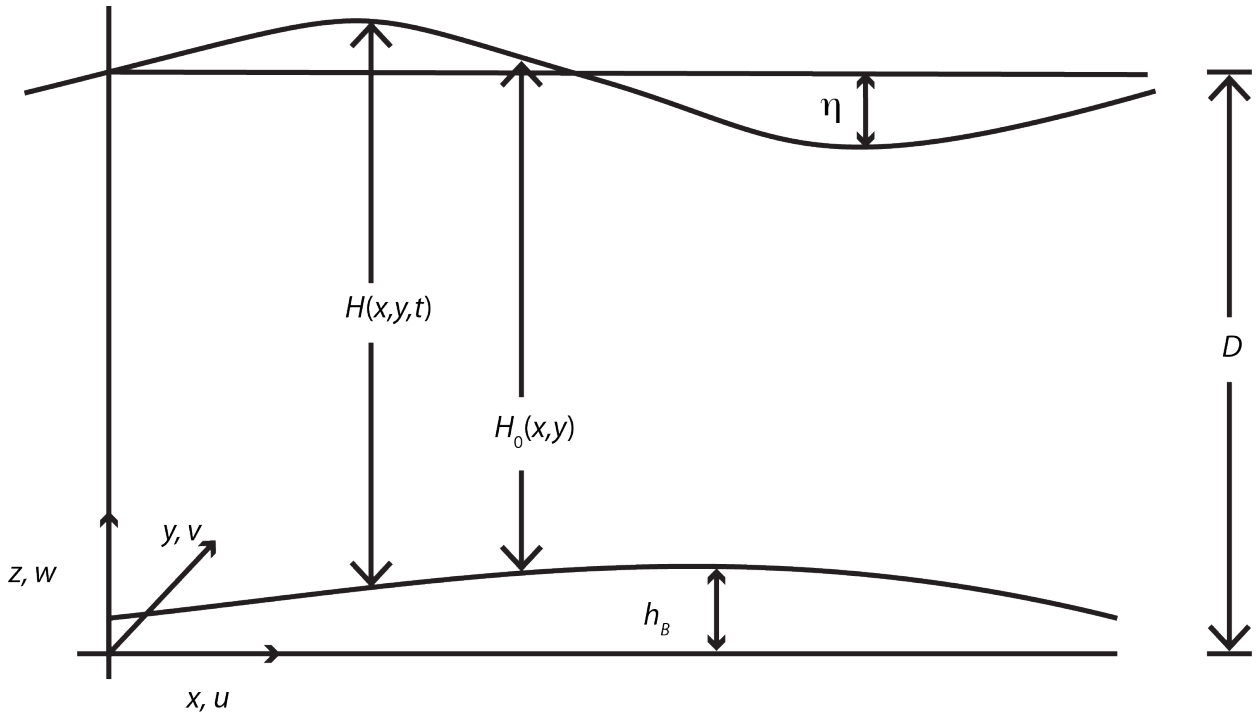

FIG. 4. Schematic of the one layer model where η is the sea surface elevation, H is the total depth, h_B is the bottom variation and D is a reference depth.

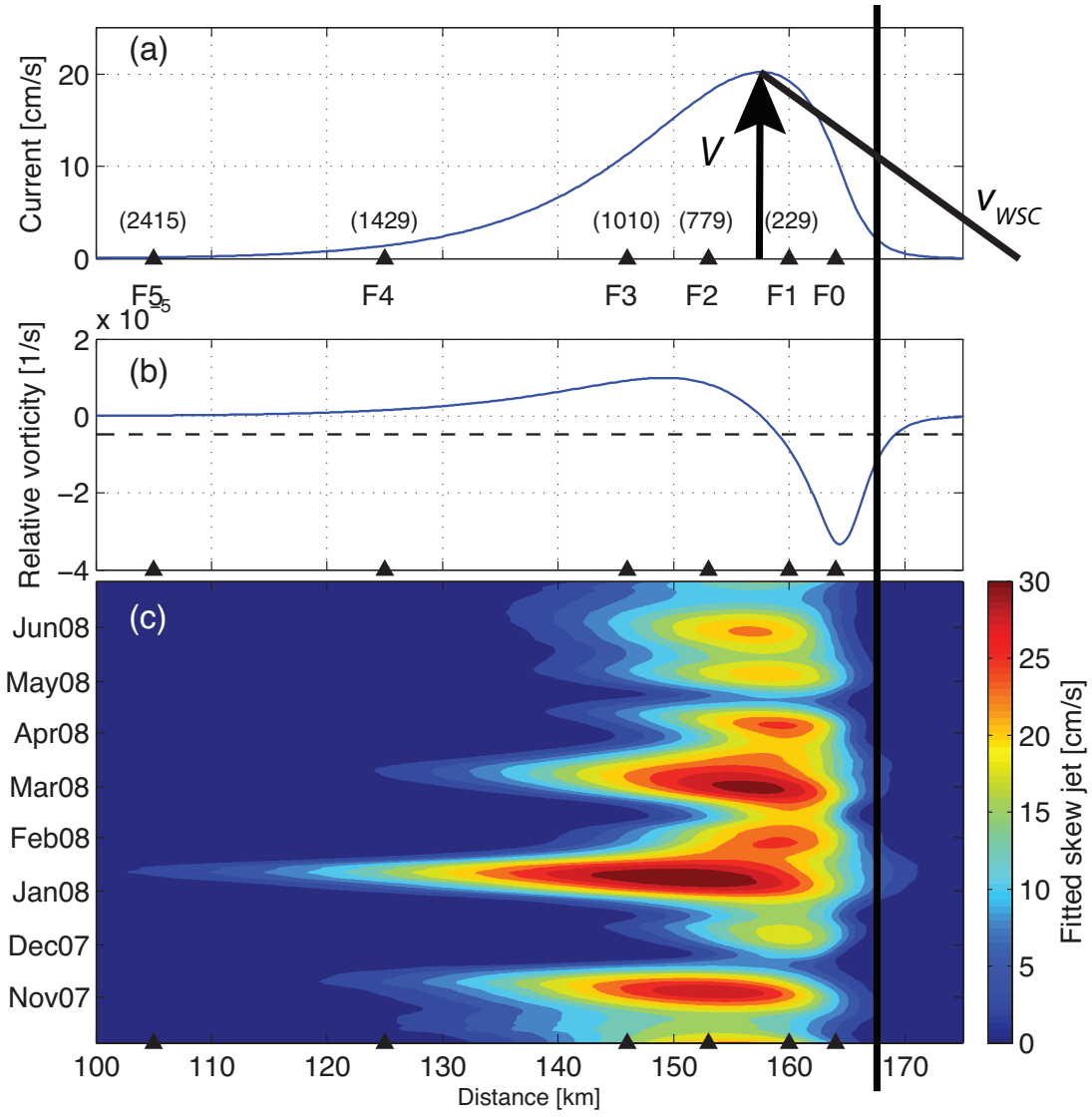

FIG. 5. The time averaged (October 2007-June 2008) velocity profile (a) of the fitted skewed jet WSC profile construct from observations in the WSC across Fram Strait at 78.83^{o}N. The black arrow shows the maximum velocity in the WSC and the line marked by v_{WSC} is the function used to represent the WSC in the model. The calculated relative vorticty of the WSC is also shown (b). A fitted skew jet profile of the WSC, from October 2007 to June 2008, at the 200-250 m level at F0-F5, from Teigen et al. (2010). Mooring positions are marked in all figures and the mooring depth is given in brackets in (a). The vertical black line through all the subfigures marks the value chosen for the relative vorticity ζ_0 in the model.

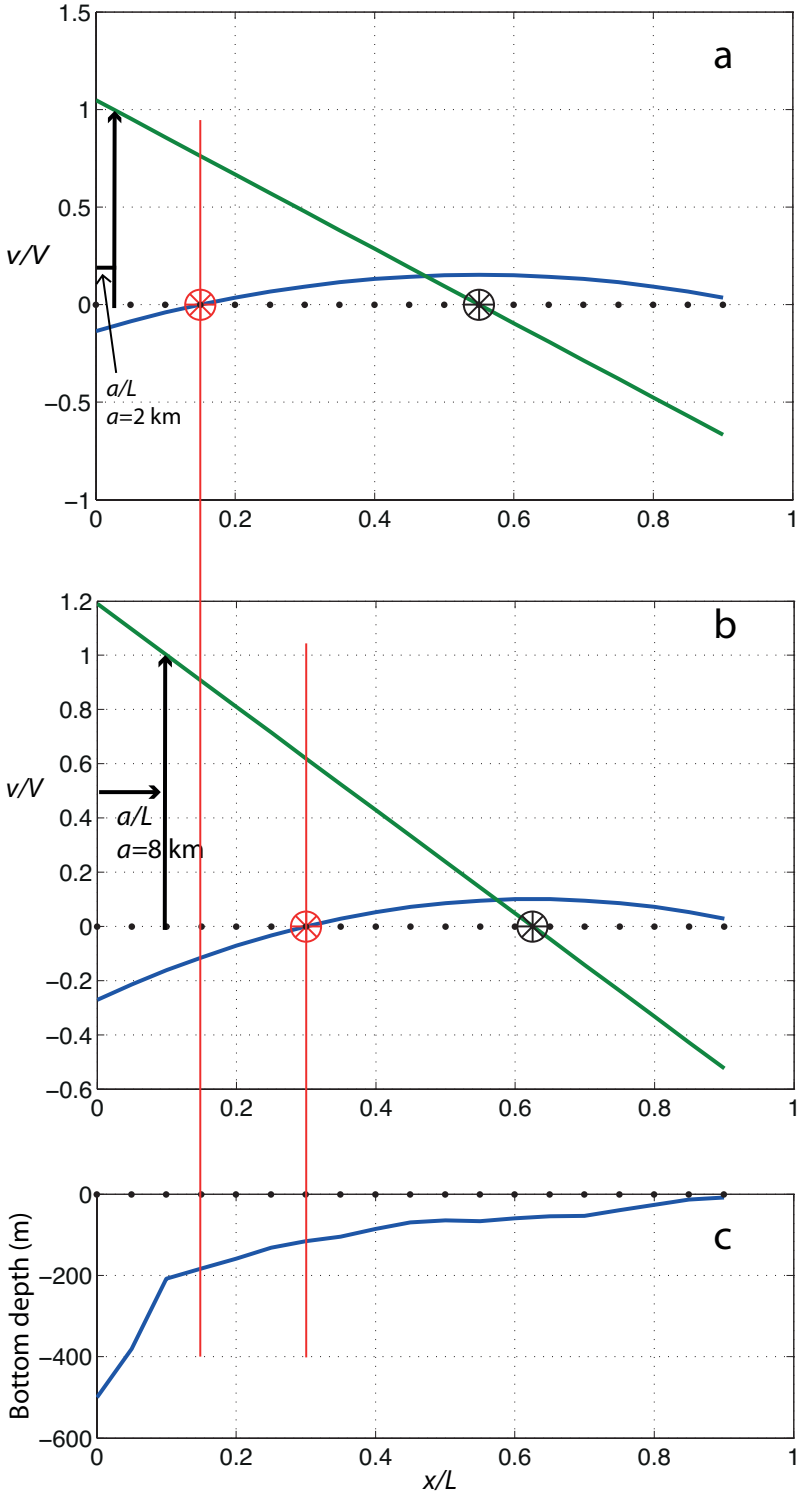

FIG. 6. The surface elevation (blue line) and corresponding WSC current (green line) representation in the barotropic model. The WSC current is moved eastward with $a = 2$ km in (a) and $a = 8$ km in (b) and the red line in each subfigure indicates the region on the WSS slope (c) that is affected by the WSC. The bottom profile in (c) represents the southern boundary of the model area where the WSC profile is prescribed. Black dots show the model grid and the vertical arrows show the position of the maximum WSC velocity.

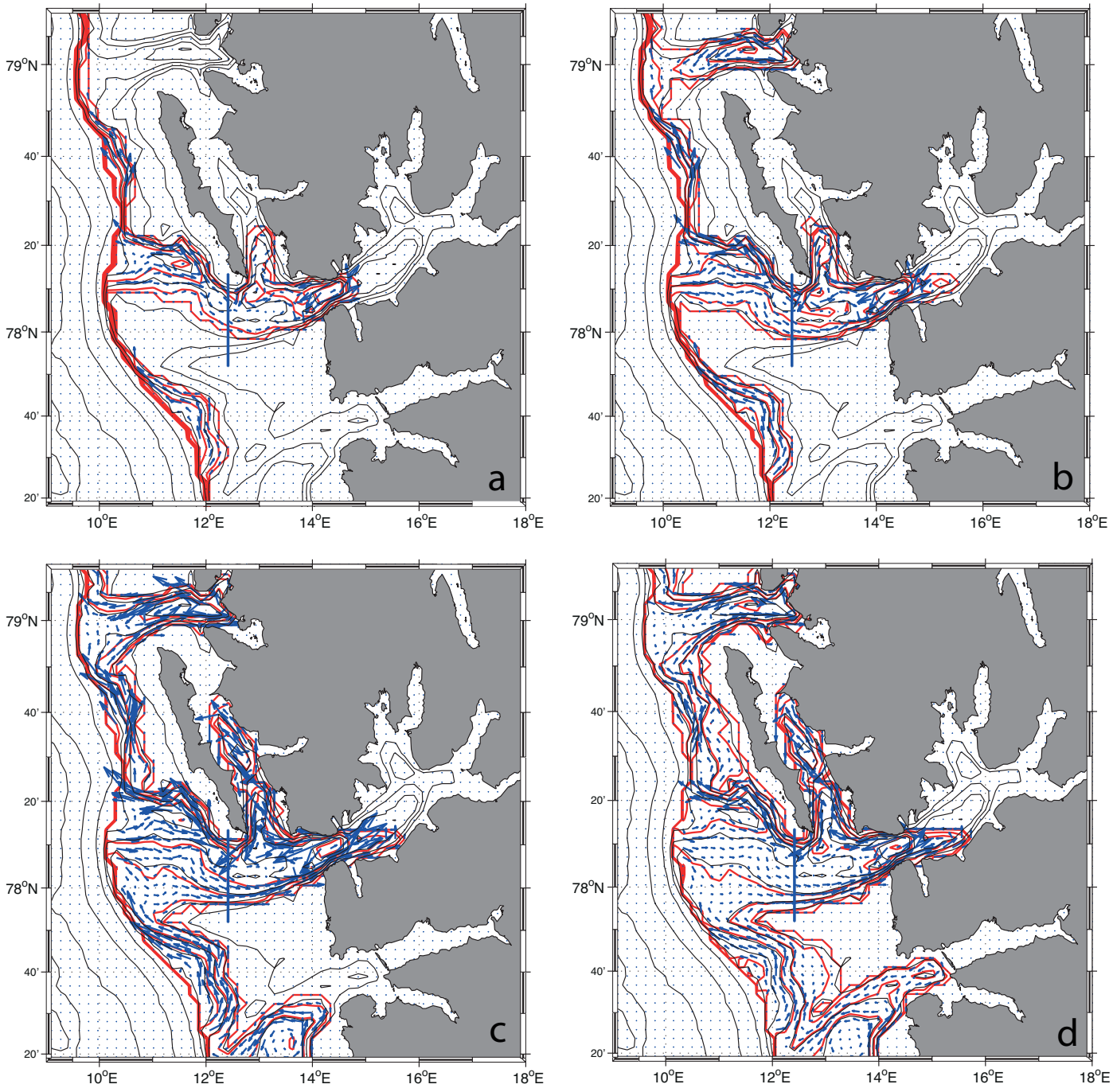

FIG. 7. The modeled circulation (a), (b), (c) and (d) where the maximum current of the WSC is translated an eastward distance a =2 km , 3 km , 8 km , and 14 km, respectively. Contoured streamlines/circulation pattern ψ (red lines) is plotted on top of the bottom topography (black lines).

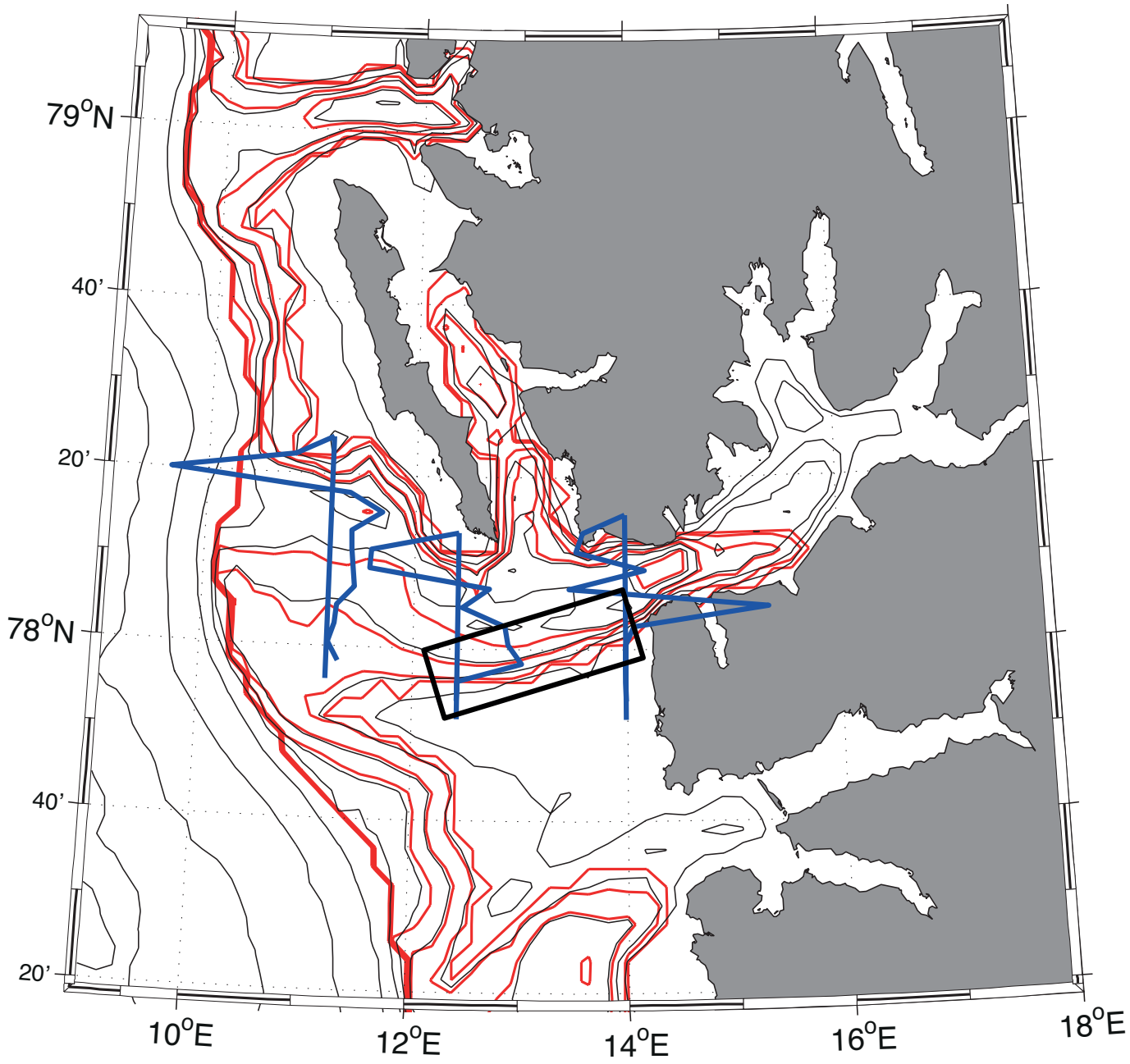

FIG. 8. Contoured streamlines/circulation pattern ψ (red lines) on top of the bottom topography (black lines). The blue curves show the volume transport across three different sections in the Isfjorden Trough when $a = 8$ km. The black rectangle marks a test area of approximately 200 km^2 that is used to calculate the effect of heat loss form the ocean to the atmosphere.